A femtosecond Raman generator for long wavelength two-photon and third harmonic generation imaging

J. Trägårdh, J. Schniete, M. Parsons, and G. McConnell

Citation: APL Photonics **1**, 091303 (2016); doi: 10.1063/1.4962207
View online: http://dx.doi.org/10.1063/1.4962207
View Table of Contents: http://scitation.aip.org/content/aip/journal/app/1/9?ver=pdfcov
Published by the AIP Publishing

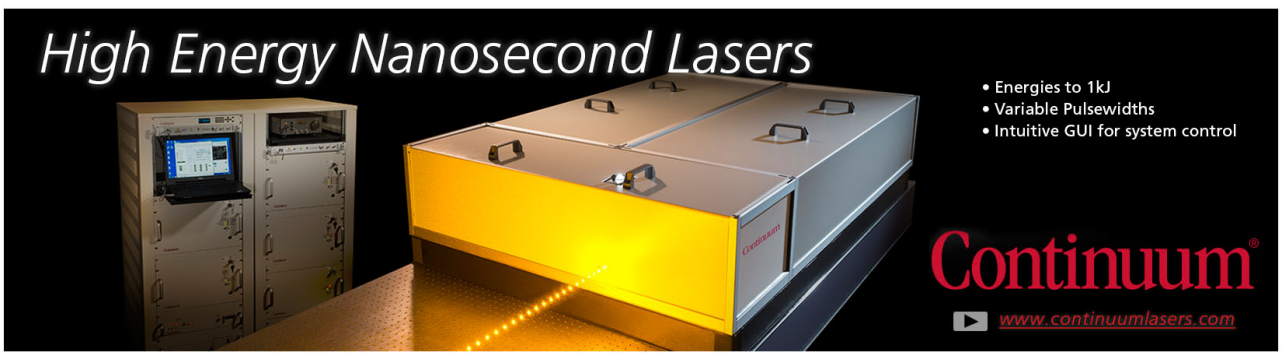

APL PHOTONICS **1**, 091303 (2016)

A femtosecond Raman generator for long wavelength two-photon and third harmonic generation imaging

J. Trägårdh,[1,a] J. Schniete,[1] M. Parsons,[2] and G. McConnell[1]
[1]*Centre for Biophotonics, SIPBS, University of Strathclyde, 161 Cathedral Street, Glasgow G4 0RE, United Kingdom*
[2]*Randall Division of Cell and Molecular Biophysics, King's College London, Guy's Campus, London SE11 UL, United Kingdom*

(Received 9 May 2016; accepted 23 August 2016; published online 27 September 2016)

We demonstrate a femtosecond single pass Raman generator based on an YVO_4 crystal pumped by a high energy fiber laser at a wavelength of 1064 nm and a repetition rate of 1 MHz. The Raman generator shifts the pump wavelength to 1175 nm, in a broadband spectrum, making it suitable for multi-photon microscopy. We use the Raman generator for third harmonic generation imaging of live plant specimens as well as for two-photon fluorescence imaging of red fluorescent protein expressing HeLa cells. We demonstrate that the photo-damage to a live specimen is low. [http://dx.doi.org/10.1063/1.4962207]

Multi-photon imaging is used for biological specimens due to its much larger penetration depth compared to single photon imaging,[1] intrinsic sectioning capability, and low out of plane photo-bleaching.[2] One mode of multi-photon imaging is third harmonic generation (THG) imaging, which allows label-free visualization of, for example, blood vessels and red blood cells,[3] and lipid structures.[4] The latter are highly important as lipid structures and droplets are key components in a number of disease conditions such as diabetes, atherosclerosis, and neurodegeneration by loss of myelination of axons.[5]

For THG imaging, it is crucial to have access to ultrashort excitation pulses at longer wavelengths than those available with a Ti:sapphire laser (>1080 nm), the most commonly used laser for nonlinear microscopy. These longer wavelengths are crucial since the detected wavelength is otherwise in the UV wavelength range, where standard microscope optics as well as the tissue itself has low transparency.

Longer excitation wavelengths would also allow more efficient excitation of fluorescence from red-emitting dyes and fluorescent proteins, e.g., Alexa 647[1] and red fluorescent protein (RFP),[6] as well as red-emitting calcium indicators. Such red-emitting dyes are increasingly being used for bio-imaging since they facilitate fluorescence imaging with multiple labels as well reduce interference from tissue autofluorescence.[6]

In this letter we report a single pass Raman generator (SPRG) based on yttrium orthovanadate (YVO_4), pumped at 1064 nm by a 1 μJ pulse energy, ultrafast fiber laser at 1 MHz. The YVO_4 crystal has a Raman frequency of 890 cm^{-1},[7] shifting the wavelength of the pump to 1175 nm by stimulated Raman scattering (SRS) in the crystal. SRS has previously been used for frequency conversion of ps and longer pulses[7–9] as well as fs pulses,[10–13] by constructing Raman generators,[7–9,12,13] amplifiers,[7,10,11] and lasers.[14,15] For fs pulses, the pulse length is less than the dephasing time (1/Raman linewidth) of the Raman material, which is a few ps for most Raman crystals,[15] and in this so-called transient regime, the Raman gain is low. Here, the short pump pulses allow competing nonlinear mechanisms, e.g., self-phase modulation, to broaden the spectrum substantially, which can be useful for imaging applications. The SPRG is the simplest of these devices

[a]Author to whom correspondence should be addressed. Electronic mail: johanna.tragardh@strath.ac.uk

to construct, requiring neither an alignment sensitive cavity nor synchronous pumping. SPRGs in crystals have been successfully constructed in the ps regime,[7,8] but for fs pump pulses this has only been accomplished at a low conversion efficiency (0.2%) for $KGd(WO_4)_2$[13] and in the impulsive SRS regime[12] where the bandwidth of the pump laser must be similar to the Raman shift. Both of these devices were pumped with lasers with too low repetition rate (1 kHz) to be useful for laser point-scanning imaging, since it would result in excessively long pixel dwell-times. In the SPRG presented in this letter, however, the repetition rate of the pump laser is 1 MHz, which is more suitable for imaging.

We use this SPRG for non-linear imaging, namely, two-photon fluorescence microscopy and THG microscopy. As THG is a third-order nonlinear process, the high pulse energies, due to the low repetition rate, allow for efficient signal generation[16] (see supplementary material). This is also the case for fluorescence excitation although there are indications that a somewhat higher repetition rate (about 5-10 MHz, see Ref. 17) is optimal.

Raman generators have, to our knowledge, not been used for multi-photon imaging although a Raman generator pumped by a ns pulse, emitting second Stokes radiation at 599 nm, was used for time gated one-photon fluorescence imaging in Ref. 9.

Alternatives to devices based on SRS for extending the wavelength beyond about 1080 nm are optical parametric oscillators (OPOs),[18] Cr:forsterite lasers,[19] and more recently, commercial systems tunable to ca 1300 nm.[20] These are however costly and/or challenging to build and to maintain (the cost of the SPRG described here was ca £50k). In addition, these often work at repetition rates of 10s of MHz, which is not optimal for THG microscopy, as discussed above. Erbium doped fiber lasers have been used for long wavelength imaging at their intrinsic wavelength of around 1500 nm.[21,22] Fiber lasers have also been used as pump lasers for tunable systems employed for imaging based on pumping a nonlinear optical element.[23] For 1300 nm low repetition rate fiber based OPAs are available, e.g., Ref. 24. Femtosecond optical parametric generators, which are simple to setup, emitting at suitable wavelengths for THG imaging have been demonstrated,[16,25] and also used for imaging,[16] although at longer wavelengths than used here. There is possibly a trade-off between using longer wavelengths with large penetration depth and poorer performance of standard objective lenses at long wavelengths.

A schematic of the SPRG is shown in Fig. 1(a). The a-cut YVO_4 crystal (Casix 501-060-400) was 9.6 mm long and was AR coated for 1525-1565 nm. The transmission of the crystal at 1064 nm and 1175 nm is 90% and 88%, respectively. The crystal was pumped at 1064 nm by a high-pulse-energy (1 μJ) ultrafast Yb:fiber laser (Fianium HE1060-1 μJ-fs) emitting 400-fs pulses, with 12 nm band width, at a repetition rate of 1 MHz. The pump light was focused into the YVO_4 crystal using a f = 125 mm focal length plano–convex singlet lens, and the emission was collimated using a f = 25 mm plano–convex singlet lens. The pump beam was polarized parallel to the c-axis of the crystal using a half-wave plate.

For the imaging experiments, the Raman generator output was filtered by a 1150 nm long pass filter (Thorlabs FEL1150) to remove the pump laser light and coupled into a home-built laser scanning multi-photon microscope,[16] Fig. S1 of the supplementary material. To compare the efficiency of excitation of fluorescence for the pump laser wavelength and the Raman shifted wavelength, the pump beam was also optionally coupled into the microscope and overlapped with the Raman shifted emission using a flip mirror. For comparing THG imaging with lasers with different repetition frequencies, THG images were also obtained using a commercial OPO at a wavelength of 1170 nm, pulse duration of 200 fs, a bandwidth of 25 nm, and a repetition frequency of 80 MHz (Coherent Chameleon OPOVis).

We performed two-photon fluorescence imaging of HeLa cells expressing RFP-LifeAct. The cells were maintained as previously described.[26] The cells were fixed for 20 min using 3.7% paraformaldehyde (Sigma-Aldrich) in PBS and washed twice in PBS. The coverslip was then mounted using Vectashield Hard-Set Mounting Medium (Vector Laboratories). For THG imaging, live *Spirogyra* sp. were placed in a glass dish with water, and one end was held down using a weight to stop specimen drift during imaging. For evaluating the photo-damage during imaging, hairs from a Primrose sp. stem were imaged by cutting a small piece along the stem and mounting as for the *Spirogyra* sp. above or in a small drop of water under a coverslip sealed with vacuum grease for

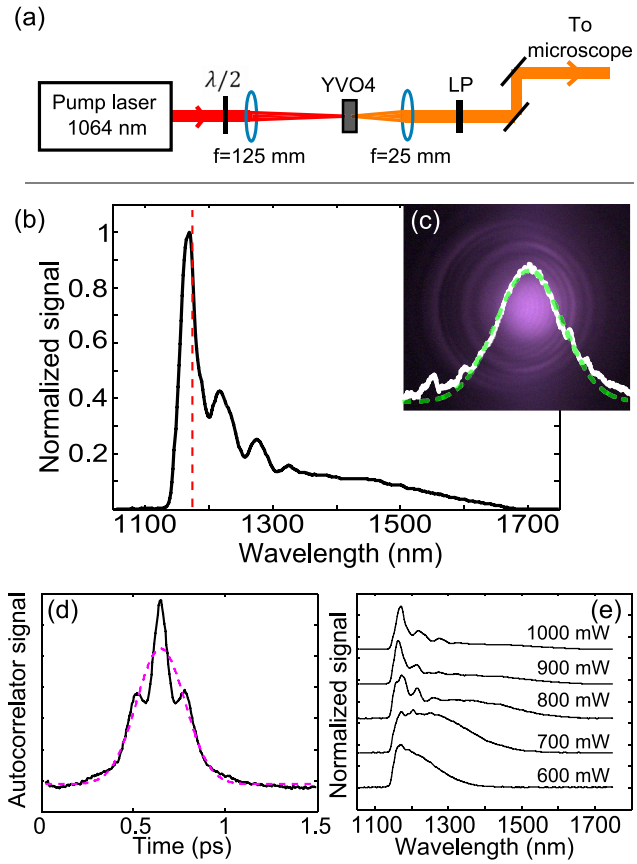

FIG. 1. (a) Schematic of the single pass Raman generator. LP = 1150 nm long pass filter. (b) Output spectrum from the Raman generator. The red dashed line indicates the expected position of the first Stokes at 1175 nm. (c) Beam profile. A cross section is shown as a solid white line and the dashed green line is a fitted Gaussian. (d) Autocorrelation trace for the SPRG. The dashed magenta line is a Gaussian fit. (e) Power dependence of the spectrum. The spectra are vertically offset for clarity.

imaging using an oil immersion objective. A small piece of a leaf of an *Elodea crispa* was mounted as for the *Spirogyra* sp. The light was focused using a Nikon Plan Apo 60× NA 1.4 oil immersion objective for imaging the RFP expressing HeLa cells and the Primrose leaf hair specimens, and a Nikon Fluor 40× NA 0.8 water dipping objective for imaging the *Spirogyra* and the *Elodea crispa* specimens. The generated two-photon fluorescence and THG signals were collected in transmission by the condenser lens (NA 0.8). The two-photon fluorescence was filtered using a 700 nm short pass filter (E700SP, Chroma Technology) and the THG signal was filtered using a 390/70 nm band-pass filter (Chroma Technologies). The signal was detected using a photomultiplier tube (Thorlabs PMM02). The image had a pixel size of 350 nm for the *Spirogyra* specimens, 300 nm for the *Elodea* specimens, and 150 nm for the RFP expressing HeLa cells and the Primrose specimens. The pixel dwell was 10 μs for the *Spirogyra* and *Elodea* specimens, and 5 μs for the RFP expressing HeLa cells and the Primrose specimen.

The output power of the Raman generator at wavelengths >1100 nm was about 25 mW, which corresponds to a conversion efficiency of 2.3%. The efficiency is likely limited by the walk-off between the pump and the Stokes pulse, which is due to the difference in refractive index at the pump and signal wavelength, rather than by the crystal length. The efficiency could possibly be improved by a double pass configuration similar to Refs. 8 and 25. The threshold was 450 mW (0.45 μJ) and the slope efficiency was 4%. The output spectrum for the Raman generator, using 1 W of pump power, is presented in Fig. 1(b). The FWHM of the spectrum was 30 nm, and the $1/e^2$ width was 160 nm for 1 W of pump power. The shape of the spectrum depended on the pump power (Fig. 1(e)). A plot of the output power as a function of pump power is shown in Fig. 2 of the

supplementary material. The high peak energy pump pulses allow competing nonlinear mechanisms (e.g., self-phase modulation) to broaden the spectrum of the Raman-shifted pump pulse substantially. The small peaks in the spectrum are possibly the interference in the crystal coating. To clarify that this was a Raman shifted spectrum, and not solely supercontinuum generation in the crystal,[27] we present the spectrum filtered using a 1100 nm LP filter in the supplementary material. We used the SPRG with 1 W pump power for all the imaging experiments. The pulse length was measured using an autocorrelator (APE Pulse Check) to be 200 fs, assuming a Gaussian pulse shape. We note that the spectrum was too wide for the bandwidth of the autocorrelator crystal, and the pulse shape is not Gaussian (Fig. 1(d)), but for these pulse lengths, the autocorrelation width/$\sqrt{2}$ is a passable estimate of the pulse width. It was not possible to compress the pulse further using a simple (SF10) prism compressor of up to 1 m in length. The beam profile was measured using a CCD camera (Thorlabs DCU223C) and was close to Gaussian (Fig. 1(c)). The output power was stable with a standard deviation in the total output power of 0.5% over 20 ms and 0.5% over 10 s.

The point spread function (psf) was measured for the 60× objective by THG imaging (using the 390/70 nm band pass filter for detection) of 500 nm diameter beads (TetraSpeck, Invitrogen T7281) mounted in Vectashield Hard-Set Mounting Medium. The lateral (axial) FWHM of the psf was 0.47 μm (1.7 μm), corrected for the bead diameter using deconvolution. To compare the psf for the pump laser and the SPRG, we also measured the psf by two-photon imaging of 500 nm diameter red-fluorescent beads (FluoSpheres F 8812, Molecular Probes). The axial FWHM of the psf was 1 μm and 1.3 μm for the pump laser and the SPRG, respectively, and the lateral FWHM of the psf for the pump laser was similar to the lateral FWHM of the psf for the SPRG. The theoretical lateral (axial) width of the psf for two-photon excitation is 210 nm (540 nm) at 1064 nm and 210 nm (600 nm) at 1175 nm.[2]

A two-photon fluorescence image of an RFP-LifeAct expressing HeLa cell is shown in Figure 2(a). The RFP-LifeAct transfection of the cells results in RFP expression in F-actin, which allows visualization of F-actin-rich cell components, such as the filopodia. The filopodia were clearly visible in the image. The time-averaged excitation power at the sample plane was 3 mW. The fluorescence intensity was about two times higher at a given excitation power for excitation at 1175 nm as compared to at the pump wavelength 1064 nm, which we attribute mainly to the difference in excitation cross section.[6] We confirmed that the contrast in the image was from a two-photon process by acquiring a series of images at different excitation powers. The slope of a linear fit to the log–log plot of the signal averaged over 15 ROI over 5 cells versus excitation power was 1.9 ± 0.2, confirming the second order excitation process.

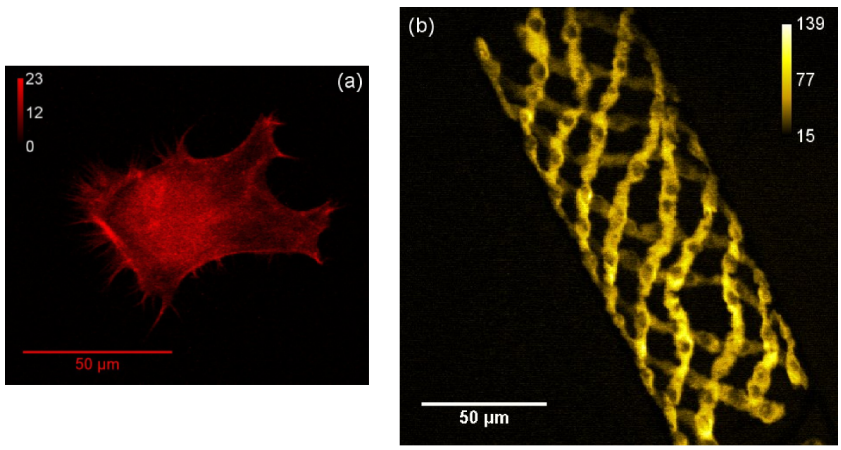

FIG. 2. (a) Two-photon fluorescence image of a RFP Life-Act expressing HeLa cell. The excitation power (at 1175 nm) was 3 mW at the sample plane. A frame average of 4 was used. (b) Average intensity projection from a z-stack (multimedia view) through a *Spirogyra* sp. imaged by THG. The excitation power was 1 mW at the sample plane. No frame averaging was used. (Multimedia view) [URL: http://dx.doi.org/10.1063/1.4962207.1]

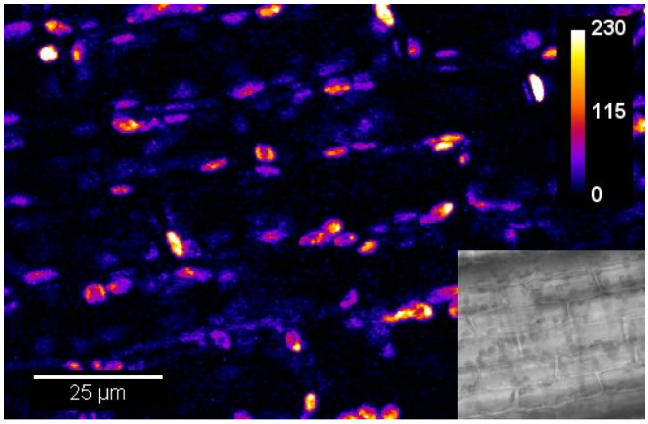

FIG. 3. THG image of cytoplasmic streaming in an *Elodea crispa* leaf (multimedia view) at the end of a 30 min imaging sequence. The excitation power was 1.2 mW at the sample plane. The inset shows a bright-field image of an *Elodea crispa* leaf showing the cell walls and chloroplasts, the latter giving the signal in the THG image. (Multimedia view) [URL: http://dx.doi.org/10.1063/1.4962207.2]

Figure 2(b) shows a THG image of a *Spirogyra* specimen. Because of the small psf, the optical sectioning is clear (multimedia view). The signal level is very high (about a third of the saturation level of the PMT) despite the low time-averaged excitation power of 1 mW. The high signal intensity at low excitation powers is a key benefit of using lower repetition rate lasers for THG imaging, since the signal level scales inversely quadratically with the repetition rate of the laser. There was no visible change of the morphology of the *Spirogyra* sp. after imaging continuously for 25 min. Comparing the required excitation power for the same signal level using an OPO at 1170 nm and 80 MHz showed that it required about 11 times higher excitation intensity, due to the different repetition rates (Fig. S4 in the supplementary material). We note that although there is no clear damage to the specimen for excitation with the OPO when using the water dipping lens, the high powers required did cause problems for samples in solid mounting media such as Vectashield or Gelvatol, when imaged using an oil immersion objective. We confirmed that the contrast in the image was from a third order process by acquiring a series of images at different excitation powers. The slope of a linear fit to the log–log plot of the signal averaged over 7 ROI over 2 *Spirogyra* sp. versus excitation power was 2.7 ± 0.2, confirming that the emission is THG.

In order to check that the high pulse energies of the laser were not causing damage to the sample, we imaged cytoplasmic streaming in an *Elodea crispa* leaf (Fig. 3). We could observe the moving chloroplasts in THG by acquiring a series of consecutive images. The cytoplasmic streaming could still be observed after 30 min of continuous imaging using an excitation power of 1.2 mW at the sample plane, indicating the low photo-damage when imaging with this laser. To investigate the photo-damage with excitation conditions more similar to those used to image the RFP expressing cells (60× oil immersion objective lens), we imaged the cytoplasmic streaming in a Primrose leaf hair, as this specimen was more compatible with imaging using the oil immersion objective, which has a short working distance. The cytoplasmic streaming (evaluated by bright field imaging) could still be observed after 20 min of continuous imaging at an excitation power of 3 mW (supplementary material).

In conclusion, we have presented multi-photon imaging with a femtosecond single pass Raman generator. The Raman generator is very easy to setup, comprising only two lenses, a filter and a $\lambda/2$ plate in addition to the pump laser, and has a low noise output. The low repetition rate allows for efficient THG and two-photon fluorescence imaging. The THG imaging is further facilitated by the long wavelength, moving the THG emission into the visible wavelength range, where the detection efficiency is increased. Finally, we have demonstrated that the photo-damage is low when imaging with this laser.

See the supplementary material for additional spectra from the Raman generator, the effect of the pump power on the output power of the SPRG, images comparing THG excitation with the OPO

and the SPRG, a description of the microscope, and a video showing bright-field imaging of the cytoplasmic streaming in a Primrose leaf hair.

This research was funded by Medical Research Council (MRC) (Grant No. MR/K015583/1) and Medical Research Scotland (Grant No. Vac-802-2015). We thank Photonic Solutions Ltd. for the loan of an auto-correlator FROG crystal. The dataset associated with this research is available at http://pure.strath.ac.uk.

[1] D. Kobat, M. E. Durst, N. Nishimura, A. W. Wong, C. B. Schaffer, and C. Xu, Opt. Express **17**, 13354 (2009).
[2] W. R. Zipfel, R. M. Williams, and W. W. Webb, Nat. Biotechnol. **21**, 1369 (2003).
[3] S. Dietzel, J. Pircher, A. K. Nekolla, M. Gull, A. W. Brändli, U. Pohl, and M. Rehberg, PLoS One **9**(6), e99615 (2014).
[4] D. Débarre, W. Supatto, A.-M. Pena, A. Fabre, T. Tordjmann, L. Combettes, M.-C. Schanne-Klein, and E. Beaurepaire, Nat. Methods **3**, 47–53 (2006).
[5] D. J. Murphy and J. Vance, Trends Biochem. Sci. **24**, 109 (1999).
[6] M. Drobizhev, N. S. Makarov, S. E. Tillo, T. E. Hughes, and A. Rebane, Nat. Methods **8**, 393 (2011).
[7] Y. Xu, M. Chen, L. Chen, C. Yang, and G. Li, Optik **125**, 545 (2014).
[8] P. Černý and H. Jelínková, Opt. Lett. **27**(5), 360 (2002).
[9] Y. Y. Hui, L.-J. Su, O. Y. Chen, Y.-T. Chen, T.-M. Liu, and H.-C. Chang, Sci. Rep. **4**, 5574 (2014).
[10] O. V. Buganov, A. S. Grabtchikov, Y. I. Malakhov, Y. M. Popov, V. A. Orlovich, and S. A. Tikhomirov, Laser Phys. Lett. **9**, 786 (2012).
[11] M. Zhi and A. V. Sokolov, New J. Phys. **10**, 025032 (2008).
[12] A. S. Grabtchikov, R. V. Chulkov, V. A. Orlovich, B. I. Stepanov, M. Schmitt, R. Maksimenko, and W. Kiefer, Opt. Lett. **28**(11), 926 (2003).
[13] V. A. Orlovich, Y. I. Malakhov, Y. M. Popov, D. N. Busko, M. B. Danailov, A. A. Demidovich, P. A. Apanasevich, and R. V. Chulkov, Laser Phys. Lett. **9**(11), 770 (2012).
[14] M. Murtagh, J. Lin, R. P. Mildren, G. McConnell, and D. J. Spence, Opt. Express **23**, 15504 (2015).
[15] J. A. Piper and H. M. Pask, IEEE J. Sel. Top. Quantum Electron. **13**, 692 (2007).
[16] J. Trägårdh, G. Robb, K. K. E. Gadalla, S. Cobb, C. Travis, G.-L. Oppo, and G. McConnell, Opt. Lett. **40**, 3484 (2015).
[17] L.-C. Cheng, N. G. Horton, K. Wang, S.-J. Chen, and C. Xu, Biomed. Opt. Express **5**, 3427 (2014).
[18] G. Norris, R. Amor, J. Dempster, W. B. Amos, and G. McConnell, J. Microsc. **246**, 266 (2012).
[19] C. K. Sun, S. W. Chu, S. Y. Chen, T. H. Tsai, T. M. Liu, C. Y. Lin, and H. J. Tsai, J. Struct. Biol. **147**(1), 19 (2004).
[20] For example Spectraphysics "InSight DS" or Coherents "Chameleon Discovery."
[21] A. C. Millard, P. W. Wiseman, D. N. Fittinghoff, K. R. Wilson, J. A. Squier, and M. Müller, Appl. Optics **38**, 7393 (1999).
[22] K. Kieu, S. Mehravar, R. Gowda, R. A. Norwood, and N. Peyghambarian, Biomed. Opt. Express **4**, 2187 (2013).
[23] N. G. Horton, K. Wang, D. Kobat, C. G. Clark, F. W. Wise, C. B. Schaffer, and C. Xu, Nat. Photonics **7**, 205 (2013).
[24] Femtosecond Optical Parametric Amplifier "Bodega," Calmar Lasers, Palo Alto, CA, USA.
[25] H. Linnenbank and S. Linden, Opt. Express **22**, 18072 (2014).
[26] A. Jayo, M. Parsons, and J. C. Adams, BMC Biol. **10**, 72 (2012).
[27] M. Bradler, P. Baum, and E. Riedle, Appl. Phys. B **97**, 561 (2009).